Published in final edited form as:
Biochemistry. 2011 April 5; 50(13): 2691–2700. doi:10.1021/bi2000966.

Rational Approach to Select Small Peptide Molecular Probes Labeled with Fluorescent Cyanine Dyes for in vivo Optical Imaging

Mikhail Y. Berezin[a], **Kevin Guo**[a], **Walter Akers**[a], **Joseph Livingston**[a], **Metasebya Solomon**[a,b], **Hyeran Lee**[a], **Kexian Liang**[a], **Anthony Agee**[a], and **Samuel Achilefu**[a,b,c,*]

[a] Department of Radiology, Washington University, St. Louis, MO 63110

[b] Department of Biomedical Engineering, Washington University, St. Louis, MO 63110

[c] Department of Biochemistry & Molecular Biophysics, Washington University, St. Louis, MO 63110

Abstract

We demonstrate that the structure of carbocyanine dyes, which are commonly used to label small peptides for molecular imaging, and not the bound peptide, controls the rate of extravasation from blood vessels to tissue. By examining several near-infrared (NIR) carbocyanine fluorophores, we demonstrate a quantitative correlation between the binding of a dye to albumin, a model plasma protein, and the rate of extravasation of the probe into tissue. Binding of the dyes was measured by fluorescence quenching of the tryptophans in albumin and was found to be inversely proportional to the rate of extravasation. The rate of extravasation, determined by kurtosis from longitudinal imaging studies using rodent ear models, provided a basis for quantitative measurements. Structure-activity studies aimed at evaluating a representative library of NIR fluorescent cyanine probes showed that hydrophilic dyes with binding constants several orders of magnitude lower than their hydrophobic counterparts have much faster extravasation rate, establishing a foundation for rational probe design. The correlation provides a guideline for dye selection in optical imaging and a method to verify if a certain dye is optimal for a specific molecular imaging application

Keywords

near-infrared; contrast agent; extravasation; kurtosis; protein binding

The development of a molecular probe in optical imaging is a complex process that requires substantial and concerted efforts from different disciplines, including chemistry, biology, physics, and engineering. From a chemistry point of view, a typical probe for molecular imaging consists of a targeting moiety, such as peptides, oligosaccharides, small organic molecules and a covalently linked fluorophore. Probes designed for deep tissue and non-invasive optical imaging are different from those for in vitro or cellular studies where desirable features include good fluorescence intensity in the visible range and decent cell

Address correspondence to: Samuel Achilefu, Ph.D. Department of Radiology, Washington University School of Medicine, 4525 Scott Avenue, Saint Louis, MO 63110, Telephone: 314-362-8599, Fax: 314-747-5191, achilefus@mir.wustl.edu.

SUPPORTING INFORMATION AVAILABLE

Quenching of tryptophan by ICG, double logarithmic plot of ICG binding to BSA, relative fluorescence as a function of dye concentration of ICG in HSA, fluorescence decays and instrument response function of the model of kurtosis, and a complete authors listing of reference [3]. This material is available free of charge via the Internet at http://pubs.acs.org.

permeability. To achieve the highest contrast between a target tissue and its surrounding for in vivo imaging, two considerations are important. First, an optical probe should preferably absorb and emit in the near infrared (NIR) region between 700 and 900 nm to facilitate light penetration from the source through tissue and back to the detector with minimal interference by endogenous absorbers (1,2). Second, the pharmacological profiles of the probe such as the rate of extravasation and clearance pathways are critical factors to minimize background fluorescence (3,4). For example, if the probe does not extravasate, targeting a non-vascular tissue becomes difficult (5) no matter how high the affinity of the probe is to the target. These considerations impose certain criteria on the design of the optical probe.

Traditionally, probe design has focused on the nature and biological activity of the targeting group and the spectral characteristics of the dye (6) but the influence of the fluorophore itself in biodistribution is usually given a secondary consideration. This strategy is reasonable because earlier reports of receptor-targeted optical imaging studies relied on antibodies as delivery vehicles to a target tissue. These biomolecules are large relative to the dye labels and their receptor specificity is well established. As a result, the primary requirement for a fluorophore was a strong fluorescent signal under biological conditions in the NIR region. With the recent development of novel synthetic methodologies, diverse functionally active fluorophores such as carbocyanines have become available (7,8). When labeled with these dyes, the inherent biological properties of the biomolecules are expected to determine the in vivo behavior of the molecular probes. However, the need to control the biodistribution profiles of optical imaging probes in vivo and the availability of high affinity small peptides have led to a proliferation of NIR fluorescent molecular probes consisting of small peptides labeled with cyanine dye. In this situation, the dye properties will affect the biodistribution of the peptide, especially if the molecular weight of the peptide is less than twice that of the dye. Accordingly, establishing selection criteria for appropriate fluorophores for in vivo applications is essential.

Herein, we report an approach for fluorophore selection based on its binding affinity to plasma proteins, particularly albumin. We hypothesized that strong binding of a fluorescent probe to albumin alters the pharmacokinetics of the probe, resulting in reduced diffusion into tissues and poor target contrast. We restricted our study to NIR fluorescent carbocyanine dyes and their small peptide conjugates. The dyes and peptides typically have molecular weights of <800 Da and 1500 Da, respectively. At present, this group of molecular probes is commonly used as in vivo imaging agents. Our results demonstrate that the fluorophore, and not the targeting moiety conjugated to the probe, is predominantly responsible for albumin binding. By examining several NIR fluorophores with structural similarity but varying number of hydrophilic groups, we showed that the more hydrophilic dyes exhibited up to two orders of magnitude lower binding constants toward albumin than their hydrophobic counterparts. We found a direct negative correlation between binding constant of a probe to albumin in vitro and the rate of extravasation of the probe into tissue as evaluated by change of kurtosis in mouse ears using high resolution NIR optical imaging. This correlation, supported by pharmacokinetic modeling, suggests that hydrophilic dyes are better suited for imaging of tissue distal from the vasculature, while hydrophobic dyes are more appropriate for vascular imaging. Thus, binding analysis of fluorophores to plasma proteins presents a new strategy in designing optical probes for in vivo applications.

MATERIALS AND METHODS

Materials

DMSO (spectrophotometric grade), bovine serum albumin (BSA, grade agarose gel electrophoresis, 99%), human serum albumin, (HSA, grade agarose gel electrophoresis,

99%) and indocyanine green (ICG) were purchased from commercial sources. High purity water (18.2 MΩ) was used throughout the study. NIR dyes cypate, LS276 and LS288 were prepared as reported previously (7,9,10). Peptide with sequence Gly-Arg-Asp-Ser-Pro-Lys (GRDSPK) and the dye-peptide conjugates LS39, LS224 and LS296 were prepared by solid state peptide synthesis as previously published (11,12). IRdye800CW was purchased from LI-COR Biosciences.

Optical measurements

UV/Vis and fluorescence spectra of samples were recorded on a spectrophotometer and fluorometer, respectively. The fluorescence was carried out with excitation at 279 nm for tryptophan quenching study (scan 294–450 nm) and 720 nm (scan 735–950 nm) for other measurements. Fluorescence lifetime of dyes was determined using time-correlated single photon counting (TCSPC) technique with NanoLed 773 nm excitation source as described previously (13). In this study, albumin in PBS was added until no more fluorescent enhancement was observed from the dyes, an indication of complete binding.

Binding measurements

BSA was dissolved in PBS buffer (10 mM) to obtain a concentration of 0.08 mg/mL and kept as a stock solution at 4°C. The dye concentration was established from standard curves using UV/Vis spectra with the following molar absorptivities in water: cypate (ε=156,000 $M^{-1}cm^{-1}$), ICG (ε=201,000 $M^{-1}cm^{-1}$), LS276 (ε=210,000 $M^{-1}cm^{-1}$), LS288 (ε=227,000 $M^{-1}cm^{-1}$),(9,13) and IRdye800CW (ε=240,000 $M^{-1}cm^{-1}$) (14). Molar absorptivities of the parent dyes were used for the dye-peptide conjugates. For binding measurements, a solution of albumin (2 mL) was placed in a 1×1 cm quartz cuvette and titrated with dye, peptide, or dye-peptide conjugate in microliter scale increments. After each addition, the solution was stirred, allowed to equilibrate for a few minutes, and its emission spectra recorded (ex/em 279/294–450 nm).

LCMS was also used to evaluate the binding constant between peptide GRDSPK and BSA. This peptide does not have a fluorophore or labeled with a fluorescent dye, which is required to quench albumin fluorescence. Therefore, we used LCMS as an alternative method for this assay. Here, the albumin in water and the peptide pre-dissolved in DMSO/water were mixed at a ~ 1:1 mole ratio and the mixture was filtered through a 0.5 mL Amicon® centrifugal filter device with 30 kD cutoff filter (Ultrafree-MC, Millipore, Billerica, MA). The filter, composed of regenerated cellulose, has a high retention efficiency of albumin (98% by fluorescence measurements, ex/em 279/345 nm) and almost complete (>98%) permeability to the peptide as measured by LC/MS-ESI analysis. LC/MS-ESI equipped with UV-Vis (217 nm) and mass-spectrometer in positive mode was used to analyze the peptide and peptide/albumin solution prior and after filtration. A 100 mm × 4.6 mm column with isocratic flow of water with 0.1 % TFA at 0.8 mL/min was used. Peak areas at retention time 5.9 min were found to correspond to the free peptide with characteristic signals $[MH^+]$ =659 and $[MH^{2+}]$=330. Using different peptide concentrations, we established a linear relationship between the concentration of the peptide and peak area (R^2 = 0.998). Binding affinity of the peptide to albumin was conducted by comparing peak areas with and without BSA. The equivalence of the peak areas in LCMS chromatograms corresponding to the peptide level with and without albumin unequivocally confirmed that the peptide did not bind in any significant manner to the protein. This type of analysis was not applicable to dyes and dye-conjugates due to their strong affinity to the filter.

Basic principles of measuring the binding constants to albumin

Since the optical properties of tryptophan and the studied dyes do not overlap, the tryptophan fluorescence measurements are free from dye fluorescence interference. The

linear relationship between albumin emission and concentration (R^2=0.99 for concentration between 0 to 2 mg/mL) provided the necessary quantification basis to measure the binding constants. Thus, we assumed that the complexation between a NIR dye and BSA occurs according to Eq. 1.

$$BSA+nDye \rightleftarrows Dye_nBSA \tag{1}$$

n - number of binding sites on albumin

The total concentration of BSA, BSA_{total}, is the sum of the concentrations of free albumin, BSA_{free}, in solution and the bound albumin:

$$[BSA_{total}]=[BSA_{free}]+[Dye_nBSA] \tag{2}$$

Therefore, the binding constant *K* is expressed as follows:

$$K=[Dye_nBSA]/([Dye]^n[BSA_{free}]) \tag{3}$$

Combining Eqs. 2 and 3 gives:

$$([BSA_{total}]-[BSA_{free}])/[BSA_{free}]=K[Dye]^n \tag{4}$$

Concentration of $[BSA_{total}]$ could be calculated from BSA fluorescence originating from the endogenous fluorophores tryptophan. Assuming each bound molecule causes complete quenching, then relative fluorescence $(F_0 - F)/F$ is proportional to the dye concentration.

$$(F_0 - F)/F=K[Dye]^n \tag{5}$$

where F_o is the fluorescence of total BSA, *F* is the fluorescence of $[BSA_{free}]$, *K* is the binding constant, and *n* is the number of binding sites

Finally, the number of binding sites can be calculated from double logarithmic plot:

$$\log[(F_0 - F)/F]=\log F+n\log[Dye] \tag{6}$$

The number of binding sites from titration experiments can be evaluated using Eq. 6. The slope of the line generated by a double logarithmic plot for all five fluorescent dyes was close to unity at low (less than 1 mol/mol dye to albumin ratio) concentrations. This indicates that only one site on the protein molecule could be occupied at any given time and therefore the Eq. 5 could be simplified as follows:

$$(F_0 - F)/F=K[Dye] \tag{7}$$

In vivo imaging

Mice were anesthetized and maintained with isoflurane gas and placed supine on the imaging platform of the LI-COR Odyssey NIR imaging system. The ears were coated with

glycerin on the imaging surface to reduce reflected light. Excitation was performed at 685 and 780 nm. Fluorescence emission was detected simultaneously in the 700 nm and 800 nm channels for autofluorescence and dye fluorescence, respectively. Total scan time was about 6 minutes for both ears or less than 3 minutes for a single ear. After a pre-injection scan, the imaging agent was administered to the mouse by lateral tail vein. Images were acquired continuously after injection for up to 2 h, then again at 3–4 h post-injection.

Image analysis

High-resolution images of fluorescence measured from mouse ears were analyzed and color coded using NIH ImageJ software. No filtering or averaging of the data was applied. Square regions of about 45 mm^2 were selected from the center of the ear. For each region of interest (ROI), kurtosis was measured using built-in functions. Pixel values were scaled to 256 bins and plotted as pixel counts versus pixel fluorescence intensity value in arbitrary units (a.u.). Analyses of raw pixel values are reported. Kurtosis decays were analyzed by nonlinear regression using GraphPad Prism.

RESULTS

Binding affinities of NIR fluorescent probes to albumin

The choice of the dyes was driven by a hypothesis that the number of hydrophilic groups affects the binding properties of the dye and alters biological outcomes such as tissue extravasation. Previously we demonstrated that dye hydrophilicity alters excretory pathways (15). The structures of the NIR dyes used in this study are shown in Figure 1. Their photophysical properties are similar: all dyes possess high molar absorptivities in the range of 150,000–250,000 M^{-1} cm^{-1} in water, moderate quantum yields (Q=0.10–0.13 in DMSO) and similar fluorescent lifetimes (~0.9–1.2 ns in DMSO(9)). Their structures share a similar polymethine skeleton and mainly differ from each other by the presence and orientation of carboxylic and sulfonate groups. While sulfonate groups are necessary for solubility, conventional synthetic procedures require carboxylic groups for further conjugation to a targeting group such as a peptide. Combining carboxylic and sulfonate functionalities in the same molecule would generate the desired chemical (covalent bonding) and physical (hydrophilicity) properties, respectively, without compromising the desirable spectral properties. Among the dyes studied, only ICG lacks a carboxylic acid group for peptide conjugation. For targeted imaging diseased tissues such as cancer, fluorescent probes with high specificity to the abnormal tissue are required. These probes generally are composed of a covalently bound fluorophore and a recognition motif (targeting group). While the assortment of possible targeting groups ranges from small molecules to antibodies, short polypeptides with 5–15 amino acids that mimic natural peptide hormones are especially attractive (16–18).

Binding of dyes to BSA

To determine binding constants between dyes or probes to BSA, several different approaches can be employed. In this work, we utilized the change in intrinsic fluorescence of tryptophan as an indication of a binding event. BSA has two tryptophan residues, Trp-134 and Trp-212, that exhibit strong and sensitive intrinsic fluorescence at 345 nm (19). The sensitivity of tryptophans emission has been used as a technique for quantitative measuring of binding affinities (20–23). In this work, all five fluorophores (ICG, cypate, LS276, LS288 and IRdye800CW) exhibited fluorescence quenching of albumin emission until complete fluorescence cessation (see Figure S1 in the Supporting Information for a representative example). Although the binding constants could be measured by other optical techniques such as examining the optical properties of the ligands rather than the protein (24,25), we utilized tryptophan fluorescence as a unifying method for all studied compounds. This

method allowed us to determine binding constants for dye and dye-peptide conjugates as well as peptides that are not very sensitive to fluorescence measurements at room temperature. Thus, to evaluate the binding constant of NIR dyes to BSA, we monitored the fluorescence of albumin through tryptophan emission (345 nm) by titrating BSA with a dye solution of known concentration. The theoretical account of measuring binding constant as well as other equilibrium parameters such as the number of binding sites is described in Materials and Methods section.

The number of occupied binding sites from titration experiments for all five fluorescent dyes was close to unity at low (less than 1 mol/mol dye to albumin) ratio used in this study, which is typical of the amount used for in vivo imaging. An example is given in Figure S2 (see Supporting Information) where a double logarithmic plot obtained from Eq. 6 for ICG shows n = 1.012 ± 0.0212, which indicates that only one site on the protein could be occupied at one time. This finding complements our previous publications (13, 26) where we had used fluorescence lifetime measurements and molecular modeling to establish that NIR dyes could potentially bind to at least two different binding sites in albumin. Thus, the binding constants of the ligands can be evaluated from the slope of linear titration curves expressed as the relative fluorescence of tryptophan $(F_0 - F)/F$ vs. [*Dye*], where Fo is the fluorescence of total albumin, F is the fluorescence of non-bound albumin [BSAfree], and [*Dye*] is a dye concentration. These linear titration curves are shown in Figure 2 and demonstrate discernible differences between the dyes, where higher slopes indicate larger binding constants.

The strongly bound dyes, ICG and cypate, exhibited remarkably similar and large binding constants K~550,000 M^{-1} to BSA. This strong affinity was found to be conserved among albumin from different species. For example, the binding constant of ICG to human albumin (HSA) K~570,000 M^{-1} (Figure S3 in the Supporting Information) is almost identical to BSA, even though HSA has only one tryptophan (27)). The similarity between the binding constants of the hydrophilic ICG and the hydrophobic cypate was informative. The lack of correlation between hydrophobicity and binding affinities to albumin has also been noted in literature (28). Theoretically, these two molecules could be viewed as surfactant systems with well-defined hydrophobic and hydrophilic domains that render the two fluorophore systems identical for albumin binding. Considering that the hydrophilicity sulfonate or carboxylic acid groups of the dyes are distal from the chromophore core of the dyes, the results suggest that the aromatic groups of the dyes primarily mediate albumin binding. However, the impact of hydrophilicity is demonstrated by a general trend of weaker dye binding to albumin than the more hydrophobic analogues. Thus, LS288 and IRdye800CW, the two most hydrophilic dyes comprising four sulfonate and one carboxylic groups, exhibited markedly lower binding constants (K~12,700 M^{-1} and 6,100 M^{-1}) than ICG and cypate. LS276, with an intermediate number of hydrophilic groups (two sulfonate and one carboxylic groups), showed an appropriately intermediate affinity as expected (K~135,000 M^{-1}).

Binding of dye-peptide conjugates to BSA

An important concern in probe design is that the physical properties of a dye could be significantly altered after conjugation to a peptide. The peptide conjugation could also modify a dye's binding affinity to albumin. Furthermore, peptide moiety of the dye-peptide conjugates could bind to albumin independently. To evaluate the effect of peptide conjugation on the binding properties of the dyes, we prepared and determined the binding constants of several dye-peptide conjugates whose structures are shown in Table 1. GRDSPK (H_2N-Gly-Arg-Asp-Ser-Pro-Lys–OH) is a linear peptide that has shown high specificity for tumor tissue when conjugated to the NIR dye cypate (29). Octreotate (NH2-DPhe-cyclo(Cys-Tyr-DTrp-Lys-Thr-Cys)-Thr-OH) is a potent somatostatin analog clinically

used for imaging cancers associated with somatostatin receptors, which are highly expressed in many tumor types (30–32).

Steady state emission and fluorescence lifetime analysis of dye-peptide conjugates were performed to determine the primary contributor (dye or peptide) to albumin binding. As we demonstrated previously, NIR dyes exhibit a small but noticeable bathochromic shift in solvents with lower polarity and concomitant increase in the lifetime (13). Since albumin binds dyes through hydrophobic pockets, one can expect that binding will shift the emission maximum and increase the lifetime. Thus, we compared emission profiles and fluorescence decays of cypate and cypate-peptide conjugate LS39 in PBS buffer (free, unbound) and in albumin solution (bound) using large excess of albumin to ensure complete binding. The changes in emission and lifetimes induced by albumin on both probes were identical. Both compounds exhibited an 8 nm bathochromic shift (Figure 3A) and an elevated fluorescence lifetime from 0.18–0.22 ns in PBS to 0.55–0.57 ns in albumin (Figure 3B), strongly suggesting that the binding of dye-peptide conjugate occurs through the dye. The binding constant of the peptide alone was almost insignificant, with $K < 5{,}000\ M^{-1}$ (Table 1), further confirming that binding does not occur through a peptide.

Having demonstrated the major role of a dye in binding to albumin, we were not surprised to find that dye-peptide conjugates, prepared from different peptides but possessing the same fluorophore, had similar binding affinities. For example, LS39 and LS224 are cypate-labeled probes but conjugated to different peptides. Both probes exhibited comparable binding constants (Table 1). In contrast, octreotate conjugated to different dyes (LS224 or LS296) resulted in markedly different binding constants. Thus, these in vitro results suggests that the binding strength between NIR probes and albumin could be accurately predicted from the properties of the dye.

In vivo imaging and image analysis

Having established that binding of probes to albumin was primarily dependent on the dye and not the peptide, we characterized the correlation between protein binding and in vivo properties. We hypothesized that lower albumin binding affinity would translate into more rapid extravasation. Hence, in vivo imaging using the NIR fluorescent dyes was performed to assess the difference between dyes after intravenous injection. The mouse ear provided easy access to blood vessels and capillary beds, ideal for noninvasive fluorescence detection and therefore served as a source of data from high resolution images (Figure 4A and 4B). Large arteries and veins could be easily distinguished from surrounding tissues, although small capillaries could not be resolved. The background signal from intrinsic tissue fluorescence generally ranged from 1 to 5% for all post-injection images.

The kinetic curves obtained from the time resolved images during the first 40 minutes after injections of non-conjugated dyes are shown in Figure 4C. The relatively hydrophobic dyes, cypate and ICG, had similar albumin binding constants and accordingly demonstrated very similar dynamic behavior: both dyes exhibited initially high intensity fluorescence immediately followed by a quick decline in intensity after injection. The hydrophilic dyes LS288 and IRDye800CW demonstrated substantially different behavior from the hydrophobic dyes. Both their fluorescence intensities increased over time, peaking at 20–30 min after injection before decreasing. LS276, a dye with a medium binding constant, displayed an intermediate clearance profile that lay between the curves of the two extremes. Since the curves seemed to correlate with albumin binding, we developed a four-compartment pharmacokinetic model (Figure 5) that centered on the albumin binding process to explain the observed kinetic profiles.

In this model, the blood component is split into two compartments – blood with unbound probe (M_1) and probes bound to albumin (M_2) (Figure 5A). We postulate that only free probe in blood can reversibly extravasate into the tissue (M_3) while no extravasation from albumin bound probe to tissue is expected. Clearance of the probe occurs through the kidneys from M_1 or through the liver from M_2. The coupled differential equations Eqs. 8–12 were derived according to the rate law that relates reaction rates to the concentrations of the different compartments of our model (36, 37). The ordinary differential equations were then solved using ODE45 function implemented in MATLAB 7.7 (The MathWorks, Inc. Natick, MA) that uses Runge-Kutta integration method of the 4th and 5th pairs with a small step size of 0.025 (37). The ODE45 function computes $M_1[t_n]$, for example, by using the solution from the immediately preceding time point, $M_1[t_{n-1}]$.

$$\frac{d[M_1]}{dt} = -k_{12} \times [M_1](t) - k_{13} \times [M_1](t) - k_{14} \times [M_1](t) + k_{21} \times [M_2](t) + k_{31} \times [M_3](t) \quad (8)$$

$$\frac{d[M_2]}{dt} = k_{12} \times [M_1](t) - k_{21} \times [M_2](t) - k_{24} \times [M_2](t) \quad (9)$$

$$\frac{d[M_3]}{dt} = k_{13} \times [M_1](t) - k_{31} \times [M_3](t) \quad (10)$$

$$\frac{d[M_4]}{dt} = k_{14} \times [M_1](t) + k_{24} \times [\mathrm{M_2}](\mathrm{t}) \quad (11)$$

$$K = k_{12}/k_{21} \quad (12)$$

The binding constant K defined in Eq. 3 and experimentally derived through tryptophan quenching experiments could be expressed as a ratio of corresponding rate constants (Eq. 12). Thus, a high k_{12}/k_{21} value would correspond to a dye with a high albumin binding constant like cypate and ICG, a low ratio would correspond to a probe with low albumin binding constant such as the hydrophilic dyes LS288 and IRdye800CW, and the medium ratio would correspond to the intermediate probe, LS276. Since the binding constants of the dyes were ~556,000 M^{-1} (cypate), ~135,000 M^{-1} (LS276) and ~6,100 M^{-1} (IRdye800CW), we applied corresponding relative values in our modeling experiments: rate constant k_{12} was set to 25.0, 5.0, and 0.25 on an arbitrary scale for the probes with high, intermediate and low albumin binding correspondingly. For simplicity, other rate constants, were assumed to be equal with $k_{13} = k_{31} = k_{21} = k_{14} = k_{24} = 1$.

To compare the model with the experimental data presented in Figure 4C, the concentrations were converted into fluorescence intensity. The assumption that fluorescence is proportional to the concentration of the probe was not valid because of the high sensitivity of fluorescence of cyanine dyes to environmental factors such as polarity and viscosity (38). Thus, fluorescence intensity of the probe was defined as a product of the probe concentration and a cumulative environmental factor n (Eqs. 13–15). Factor n is related to quantum yield and could be indirectly estimated from lifetime measurements in vivo and in

water. Previous results showed that the lifetime of cyanine dyes increase in vivo by a factor ranging from 2.3 to 4.1 compared to water (38).

Therefore, the environmental factors of all unbound dyes were set to one (n_1=1) and tissue and blood bound dyes to the average value of 3 ($n_2 = n_3 = 3$).

$$I_{blood}=n_1 \times [M_1]+n_2 \times [M_2] \quad (13)$$

$$I_{tissue}=n_3 \times [M_3] \quad (14)$$

$$I_{total}=I_{blood}+I_{tissue} \quad (15)$$

The results of the kinetic modeling experiments remarkably reproduced the trends in kinetic curves observed in longitudinal imaging experiments (compare Figure 5B and Figure 4C) demonstrating that variability in albumin binding has a pronounced effect on the kinetic profiles of probes in vivo.

Semi-quantitative measurements of tissue extravasation from time-resolved high-resolution ear images obtained *in vivo* were assessed by kurtosis. Kurtosis is a statistical function which refers to the “flatness” of data distribution and has been applied in magnetic resonance (39) and nuclear (40) imaging methods. This function is independent of intensity and approaches zero as fluorescence from blood vessels becomes equal to extravascular space (schematically shown in Figure S4 in the Supporting Information). In this study, we applied kurtosis as an effective measure of the contrast between blood vessels and surrounding tissues and utilized the change in kurtosis as a simple way to measure the rate of extravasation. The change in kurtosis from the selected ROIs computed from different time points and expressed as kurtosis decay half-lives showed that the trend in vivo closely corroborated our established relationship in albumin binding in vitro (Figure 4D). High affinity dyes (ICG and cypate) possessed the highest kurtosis half-life and therefore the slowest rate of extravasation (6.5 and 3.86 min respectively). LS276 with its intermediate binding constant had faster kurtosis decays of 1.57 min. Finally, the low-affinity dyes (LS288 and IRdye800CW) extravasated so rapidly that the initial kurtosis values were less than 1 even at the first time point (2 min after injection) and therefore their decay half-life was taken as close to zero.

The kurtosis data for fluorophore-peptide conjugates also followed the trend established by the binding constants of dyes to albumin. Fluorescence intensity maps for LS224 and LS296 at several representative time points are shown in Figure 6A and 6D, respectively, demonstrating the dramatic difference in extravasation. LS224 maintains sharp kurtosity throughout the entire time frame Figure 6B, whereas kurtosity of LS296 clearly diminished (Figure 6E). In line with our findings described above, octreotate conjugated to the hydrophobic cypate or the hydrophilic LS276 showed the same trends in intensity as their non-conjugated parent dyes (Figure 6C, 6E). The increase in overall fluorescence intensity in the ROI area observed for LS224 over the first 2 h was similar to the increase of the parent LS276 and the sharp decline in intensity for LS296 was similar to the rapid decline of its parent cypate. This obvious similarity in kinetic behavior between the parent dyes and their conjugates confirmed that the extravasation properties of the conjugates are dictated by the properties of the parent dye, specifically by the dye’s affinity toward albumin.

DISCUSSION

Selecting the appropriate fluorophore for in vivo imaging is not straightforward as the probes differ in spectral, chemical, physical and biological characteristics. At the same time, the selection of the proper dye for imaging application is critical for obtaining bright and high contrast images. The goal of this work was to develop a guideline to assist in identifying or synthesizing optimal NIR dye for a particular optical in vivo imaging application. Such a dye, conjugated to a biologically relevant small targeting moiety such as peptides, carbohydrates, and nucleic acids, will be better suited for imaging than a randomly chosen fluorophore. Our model study focused on cyanine dyes and small peptides with molecular weights of less than 1500 Da. To achieve our goal, we developed several fundamental relationships between structures of the cyanine dyes and their imaging properties.

We determined the binding constant of dyes to albumin and established that structurally similar NIR dyes exhibited a large, two-order of magnitude range of binding affinities to serum albumin. We found a direct correlation between the number of hydrophilic groups in the dye and its binding affinity: a higher number of hydrophilic groups led to lower binding. The positioning of the hydrophilic groups was found to be important; the attachment of hydrophilic groups directly to the chromophore was critical for low binding performance. Through a variety of optical methods, we established that dye-peptide conjugates bind to albumin through the dye and not through the peptide, therefore retaining the same trend in albumin binding as their parent dyes.

We observed that upon in vivo administration, the initially high intensity fluorescence of ICG and cypate, dyes with high affinities for albumin, declined quickly, which we attributed due to fast and complete opsonization by plasma proteins. Apparently, complete opsonization occurred prior to the first time point (2 min) and therefore the sharp rise in intensity during the first two minutes was undetected. For low binding probes such as LS288 and IRdye800CW, the maximum fluorescence intensity was reached only after 20–30 min. The increase in fluorescence in the ROI was caused by slow opsonization of the probe due to low binding constants of hydrophilic dyes and a higher level of extravasation. As expected from the albumin binding study, the medium binding probe LS276 showed intermediate behavior between hydrophobic and hydrophilic dyes. Thus, the longitudinal experimental results could be reasonably explained by taking into account albumin binding. Pharmacokinetic modeling using a four-compartment model that includes albumin binding as a key component correctly described the kinetic behavior of the dyes and dyes-conjugates in vivo. The model also demonstrated that this non-specific protein binding was the major parameter that affects the extravasation of the probe.

For molecular imaging, good contrast requires interaction of the molecular probe with the target of interest. Optimization of the molecular probes can decrease the lag time between probe injection and imaging, enhance signal to noise ratio, and reduce probe dosage and potential toxicity. Contrast could be expressed in a familiar signal-to-noise ratio and measured as a ratio of fluorescence intensities from the point of interest to the background. Generally, blood vessels covering the entire area of interest are the largest contributor to background in optical imaging. Consequently, probes with high blood protein binding are expected to give more background fluorescence, confounding the signal from the tissue and affecting the quality of the images. Thus, for tissue imaging, low albumin binding dyes are optimal. In contrast, if the application requires vascular imaging, the extravasation of the probe into tissue produces significant background fluorescence. Consequently, to enhance contrast in vascular imaging, high protein binding probes are advantageous. Alternatively, relatively large nanoparticles can be used to prevent extravasation. In addition to high

contrast, the intensity of the signal from blood could also be improved. In both cases, high contrast images will be achieved in a shorter time. The graphical representation of these conclusions derived directly from a four-compartment pharmacokinetic model is shown in Figure 5C and 5D.

The ramifications of this study suggest a clear guideline for NIR cyanine dye selection in optical imaging and a method to verify if a certain dye or dye-conjugate is optimal for a specific biological application. The structures of the dyes in Figure 1 clearly suggests that disruption of the hydrophobic chromophore core with hydrophilic groups such as sulfonates (LS-288 and IRdye800CW) significantly decreased probe binding to blood proteins such as albumin. Incorporating a modifying group on the meso-position of the cyanine dye (LS276) creates dyes that bind weakly to BSA and are useful for controlled release of the imaging agent. For cancer imaging, lymph nodes mapping, inflammation detection, and other tissue specific imaging, low protein binding dyes are optimal. For blood related diseases such as acute vascular injuries, atherosclerosis, clogging, and angiogenesis, high protein binding probes are more aptly suited. The approach described in this report using protein binding constant allows the prediction of in vivo extravasation behavior based on in vitro data. Optimization of the models and protocols can conceivably minimize the number of animals used to screen optical imaging agents in vivo. Additionally, the method is applicable to drug development, where bioavailability using the model developed in this study can be used to optimize drug design. As stated above, our study focused on small peptide-cyanine dye conjugates. With large targeting groups such as antibodies, the lager component is expected to determine biodistribution profile of the molecular probes. In addition to large biomolecules, the structural features of other important classes of fluorescent labels based on synthetic dyes such as xanthene dyes, bacteriochlorophylls, phthalocyanines, lanthanide complexes, fluorescent polymer nanoparticles, and quantum dots may have different behavior and have to be evaluated separately.

Supplementary Material

Refer to Web version on PubMed Central for supplementary material.

Acknowledgments

Funding Support: This work was supported in part by research grants from the US National Institutes of Health NIBIB (R01 EB007276 and R01 EB00811) and NCI (R01 CA109754, U54 CA136398, and U54 CA119342).

References

1. Weissleder R, Ntziachristos V. Shedding light onto live molecular targets. Nat Med. 2003; 9:123–128. [PubMed: 12514725]
2. le Masne de Chermont Q, Chaneac C, Seguin J, Pelle F, Maitrejean S, Jolivet JP, Gourier D, Bessodes M, Scherman D. Nanoprobes with near-infrared persistent luminescence for in vivo imaging. Proc Natl Acad Sci U S A. 2007; 104:9266–9271. [PubMed: 17517614]
3. Kelloff GJ, Krohn KA, Larson SM, Weissleder R, Mankoff DA, Hoffman JM, Link JM, Guyton KZ, Eckelman WC, Scher HI, O'Shaughnessy J, Cheson BD, Sigman CC, Tatum JL, Mills GQ, Sullivan DC, Woodcock J. The progress and promise of molecular imaging probes in oncologic drug development. Clin Cancer Res. 2005; 11:7967–7985. [PubMed: 16299226]
4. Rosenecker J, Zhang W, Hong K, Lausier J, Geppetti P, Yoshihara S, Papahadjopoulos D, Nadel JA. Increased liposome extravasation in selected tissues: effect of substance P. Proc Natl Acad Sci U S A. 1996; 93:7236–7241. [PubMed: 8692975]
5. Kovar JL, Simpson MA, Schutz-Geschwender A, Olive DM. A systematic approach to the development of fluorescent contrast agents for optical imaging of mouse cancer models. Anal Biochem. 2007; 367:1–12. [PubMed: 17521598]

6. Adams KE, Ke S, Kwon S, Liang F, Fan Z, Lu Y, Hirschi K, Mawad ME, Barry MA, Sevick-Muraca EM. Comparison of visible and near-infrared wavelength-excitable fluorescent dyes for molecular imaging of cancer. J Biomed Opt. 2007; 12:024017. [PubMed: 17477732]
7. Lee H, Mason JC, Achilefu S. Heptamethine cyanine dyes with a robust C-C bond at the central position of the chromophore. J Org Chem. 2006; 71:7862–7865. [PubMed: 16995699]
8. Bouteiller C, Clave G, Bernardin A, Chipon B, Massonneau M, Renard PY, Romieu A. Novel water-soluble near-infrared cyanine dyes: synthesis, spectral properties, and use in the preparation of internally quenched fluorescent probes. Bioconjug Chem. 2007; 18:1303–1317. [PubMed: 17583926]
9. Lee H, Berezin MY, Henary M, Strekowski L, Achilefu S. Fluorescence lifetime properties of near-infrared cyanine dyes in relation to their structures. J Photochem Photobiol, A. 2008; 200:438–444.
10. Ye Y, Bloch S, Kao J, Achilefu S. Multivalent carbocyanine molecular probes: synthesis and applications. Bioconjug Chem. 2005; 16:51–61. [PubMed: 15656575]
11. Bloch S, Xu B, Ye Y, Liang K, Nikiforovich GV, Achilefu S. Targeting Beta-3 integrin using a linear hexapeptide labeled with a near-infrared fluorescent molecular probe. Mol Pharmaceutics. 2006; 3:539–549.
12. Bugaj JE, Achilefu S, Dorshow RB, Rajagopalan R. Novel fluorescent contrast agents for optical imaging of in vivo tumors based on a receptor-targeted dye-peptide conjugate platform. J Biomed Opt. 2001; 6:122–133. [PubMed: 11375721]
13. Berezin M, Achilefu S. Novel synthon for incorporating 1,3-dimethyl imidazolium group into molecular architecture. Tetrahedron Lett. 2007; 48:1195–1199. [PubMed: 17417670]
14. Achilefu S, Wilhelm RR, Jimenez HN, Schmidt MA, Srinivasan A. A new method for the synthesis of tri-tert-butyl diethylenetriaminepentaacetic acid and its derivatives. J Org Chem. 2000; 65:1562–1565. [PubMed: 10814125]
15. Goiffon R, Akers W, Berezin MY, Lee H, Achilefu S. Noninvasive monitoring of renal function in vivo by fluorescence lifetime imaging. J Biomed Optics. 2009; 14:020501–020503.
16. Zwanziger D, Beck-Sickinger AG. Radiometal targeted tumor diagnosis and therapy with peptide hormones. Curr Pharm Des. 2008; 14:2385–2400. [PubMed: 18781989]
17. Aina OH, Liu R, Sutcliffe JL, Marik J, Pan CX, Lam KS. From combinatorial chemistry to cancer-targeting peptides. Mol Pharmaceutics. 2007; 4:631–651.
18. Kovar JL, Volcheck W, Sevick-Muraca E, Simpson MA, Olive DM. Characterization and performance of a near-infrared 2-deoxyglucose optical imaging agent for mouse cancer models. Anal Biochem. 2009; 384:254–262. [PubMed: 18938129]
19. Johansson JS. Binding of the volatile anesthetic chloroform to albumin demonstrated using tryptophan fluorescence quenching. J Biol Chem. 1997; 272:17961–17965. [PubMed: 9218421]
20. Cheng ZJ, Zhang YT. Spectroscopic investigation on the interaction of salidroside with bovine serum albumin. J Mol Struct. 2008; 889:20–27.
21. Papadopoulou A, Green RJ, Frazier RA. Interaction of flavonoids with bovine serum albumin: a fluorescence quenching study. J Agric Food Chem. 2005; 53:158–163. [PubMed: 15631523]
22. Vekshin NL, Sukharev VI, van Hoek A, Visser AJWG. Competition between energy transfer and deactivation during quenching of tryptophan fluorescence of albumin by dye molecules. J Fluoresc. 1999; 9:99–101.
23. Wei YL, Li JQ, Dong C, Shuang SM, Liu DS, Huie CW. Investigation of the association behaviors between biliverdin and bovine serum albumin by fluorescence spectroscopy. Talanta. 2006; 70:377–382. [PubMed: 18970778]
24. Meadows F, Narayanan N, Patonay G. Determination of protein-dye association by near infrared fluorescence-detected circular dichroism. Talanta. 2000; 50:1149–1155. [PubMed: 18967810]
25. Abugo OO, Herman P, Lakowicz JR. Fluorescence properties of albumin blue 633 and 670 in plasma and whole blood. J Biomed Opt. 2001; 6:359–365. [PubMed: 11516328]
26. Berezin MY, Lee H, Akers W, Nikiforovich G, Achilefu S. Ratiometric analysis of fluorescence lifetime for probing binding sites in albumin with near-infrared fluorescent molecular probes. Photochem Photobiol. 2007; 83:1371–1378. [PubMed: 18028211]
27. He XM, Carter DC. Atomic structure and chemistry of human serum albumin. Nature. 1992; 358:209–215. [PubMed: 1630489]

28. Frazier RA, Papadopoulou A, Green RJ. Isothermal titration calorimetry study of epicatechin binding to serum albumin. J Pharm Biomed Anal. 2006; 41:1602–1605. [PubMed: 16522360]
29. Achilefu S, Bloch S, Markiewicz MA, Zhong T, Ye Y, Dorshow RB, Chance B, Liang K. Synergistic effects of light-emitting probes and peptides for targeting and monitoring integrin expression. Proc Natl Acad Sci U S A. 2005; 102:7976–7981. [PubMed: 15911748]
30. Ha L, Mansberg R, Nguyen D, Bui C. Increased activity on In-111 octreotide imaging due to radiation fibrosis. Clin Nucl Med. 2008; 33:46–48. [PubMed: 18097260]
31. Koopmans KP, Jager PL, Kema IP, Kerstens MN, Albers F, Dullaart RP. 111In-octreotide is superior to 123I-metaiodobenzylguanidine for scintigraphic detection of head and neck paragangliomas. J Nucl Med. 2008; 49:1232–1237. [PubMed: 18632829]
32. Rufini V, Calcagni ML, Baum RP. Imaging of neuroendocrine tumors. Semin Nucl Med. 2006; 36:228–247. [PubMed: 16762613]
33. Achilefu S, Bloch S, Markiewicz MA, Zhong T, Ye Y, Dorshow RB, Chance B, Liang K. Synergistic effects of light-emitting probes and peptides for targeting and monitoring integrin expression. Proc Natl Acad Sci U S A. 2005; 102:7976–7981. [PubMed: 15911748]
34. Achilefu S, Dorshow RB, Bugaj JE, Rajagopalan R. Novel receptor-targeted fluorescent contrast agents for in vivo tumor imaging. Invest Radiol. 2000; 35:479–485. [PubMed: 10946975]
35. Achilefu S, Jimenez HN, Dorshow RB, Bugaj JE, Webb EG, Wilhelm RR, Rajagopalan R, Johler J, Erion JL. Synthesis, in vitro receptor binding, and in vivo evaluation of fluorescein and carbocyanine peptide-based optical contrast agents. J Med Chem. 2002; 45:2003–2015. [PubMed: 11985468]
36. Butcher, JC. Numerical Methods for Ordinary Differential Equations. 2. Wiley; Chichester, England: 2003.
37. Cutlip, MB.; Shacham, M.; Cutlip, MB. Safari Books Online (Firm). Problem solving in chemical and biochemical engineering with POLYMATH, Excel, and MATLAB. 2. Prentice Hall; Upper Saddle River, N.J: 2007.
38. Akers WJ, Berezin MY, Lee H, Achilefu S. Predicting in vivo fluorescence lifetime behavior of near-infrared fluorescent contrast agents using in vitro measurements. J Biomed Opt. 2008; 13:054042. [PubMed: 19021422]
39. Jensen JH, Helpern JA, Ramani A, Lu H, Kaczynski K. Diffusional kurtosis imaging: the quantification of non-gaussian water diffusion by means of magnetic resonance imaging. Magn Reson Med. 2005; 53:1432–1440. [PubMed: 15906300]
40. Itti E, Fauroux B, Pigeot J, Isabey D, Clement A, Evangelista E, Harf A, Meignan M. Quantitative lung perfusion scan as a predictor of aerosol distribution heterogeneity and disease severity in children with cystic fibrosis. Nucl Med Commun. 2004; 25:563–569. [PubMed: 15167515]

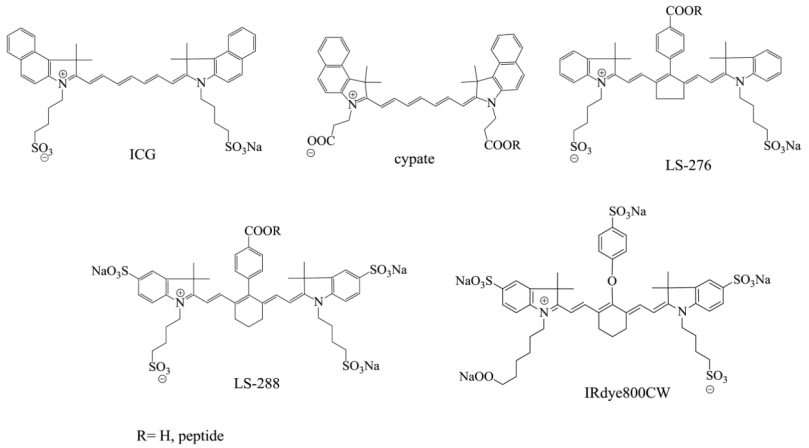

FIGURE 1.
Structures of NIR fluorescent probes used in this study

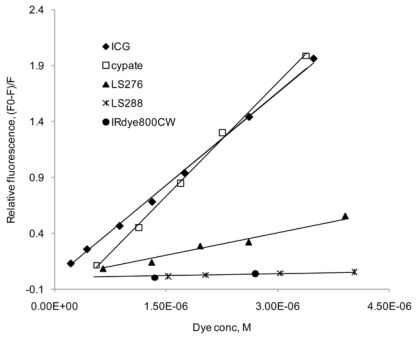

FIGURE 2.

Relative fluorescence as a function of dye concentration (ex/em 279/345nm, BSA conc. 1.4 × 10−6 M in PBS). Slope of the trend lines corresponds to the binding constants. ICG and cypate possess the strongest binding constant to albumin with values of 554,000 and 556,000 M−1 correspondingly, followed by LS276 (135,000 M−1); LS288 and IRDye800 CW bind the weakest (12,100 and 6,100 M−1 correspondingly).

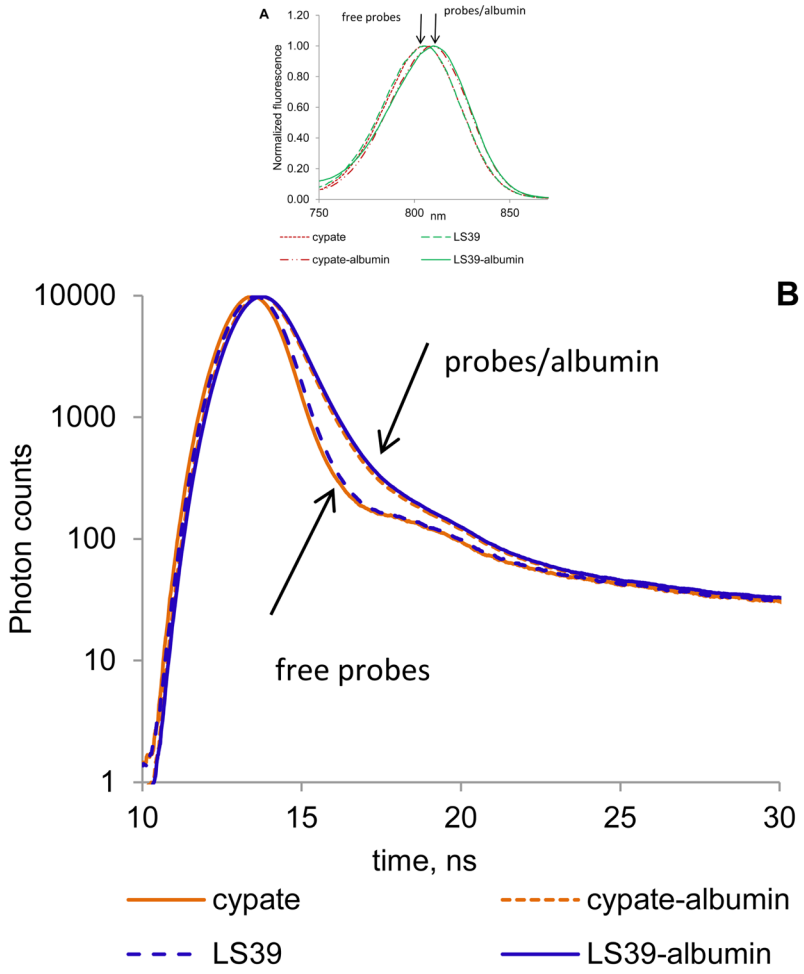

FIGURE 3.

(A) Normalized fluorescence of cypate and LS39 in PBS buffer (free probes) and albumin/PBS buffer (probe/albumin) (ex/em 720/735–900 nm). (B) Fluorescence lifetime decays of probes in PBS buffer (free) and albumin/PBS solution (bound) (ex/em.773/820 nm). Lifetimes: cypate/PBS – 0.18 ns, cypate/PBS/albumin – 0.55 ns average, LS39/PBS – 0.22 ns, LS39/PBS/albumin – 0.57 ns average. Both probes have identical spectra and lifetimes in albumin indicating the same microenvironment around the fluorophore.

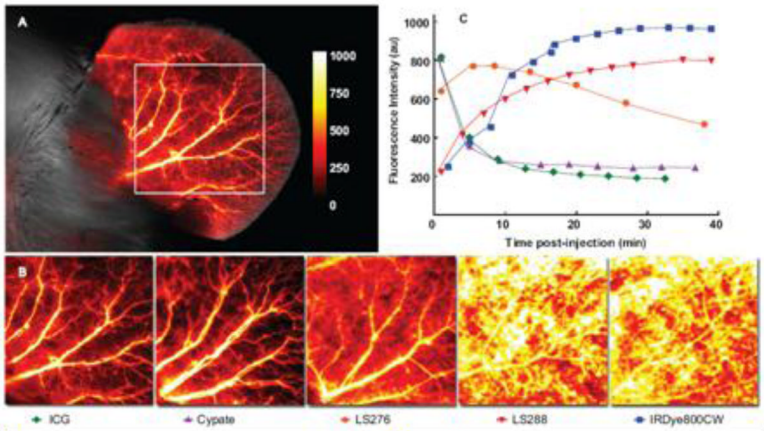

D		Binding constants		
554,000	556,000	135,000	12,700	6,100
		Kurtosis decay half-life (min)		
6.50	3.86	1.57	0	0

FIGURE 4.

High resolution fluorescence intensity map of mouse ear immediately (<2 min) after injection of NIR fluorescent contrast agents of ICG (***A***) and other dyes including ICG (***B***), ex/em 780/800 nm. Autofluorescence signal from the 700 nm channel is shown in grayscale; the enboxed area was used for kurtosis analysis. Background signal as measured by pre-injection image was subtracted from the above images and was generally less than 5% of signal. Images demonstrate the differences in extravasation of dyes: more hydrophobic dyes extravasate much faster. (***C***) Fluorescence intensity decay curves for NIR fluorescent dyes from the ROIs shown in (*B*). Fluorescence intensity displayed on the y-axis represents the sum average of the signal in the ROI.

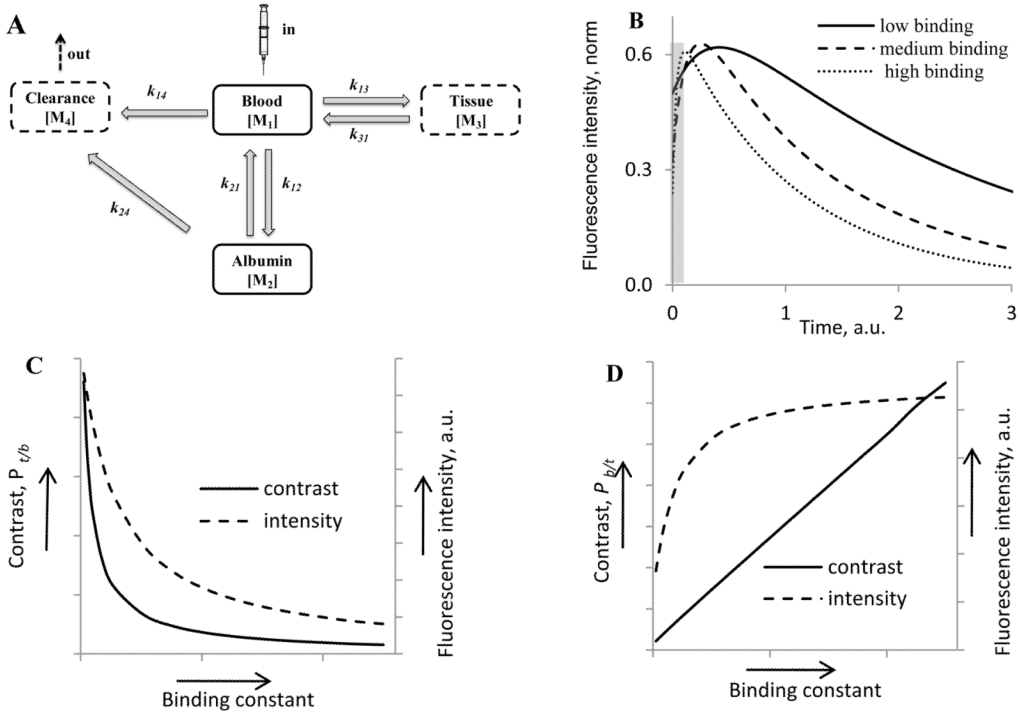

FIGURE 5.

Four-compartment pharmacokinetic model of probes for optical imaging; **(*A*)** Schematics of the model; (***B***) Kinetic curves of probes with different binding constants obtained using a four compartment model. Fluorescence intensity represents a sum of M_1, M_2 and M_3 values. Grey area corresponds to the "void" time of 2 min prior to the first measurement. k_{12} was set to 25.0 (high binding), 5.0 (medium binding), and 0.25 (low binding), $k_{13} = k_{31} = k_{21} = k_{14} = k_{24} = 1$; $n_1=1$, $n_2=n_3=3$. (***C, D***) Tissue contrast $P_{t/b}(t)=I_{tissue}(t)/I_{blood}(t)$, blood contrast, $P_{b/t}(t)=I_{blood}(t)/I_{tissue}(t)$ and intensity signals for tissue and blood as a function of binding constants. The curves are derived from a four-compartment pharmacological model. Low binding constant probes provide higher intensity signals and higher contrast for tissue imaging (***C***), while high binding constant provide better signal and contrast for blood vessels imaging (***D***). The data were obtained from numerical solutions of Eqs. 8–15 using the proposed kinetic model.

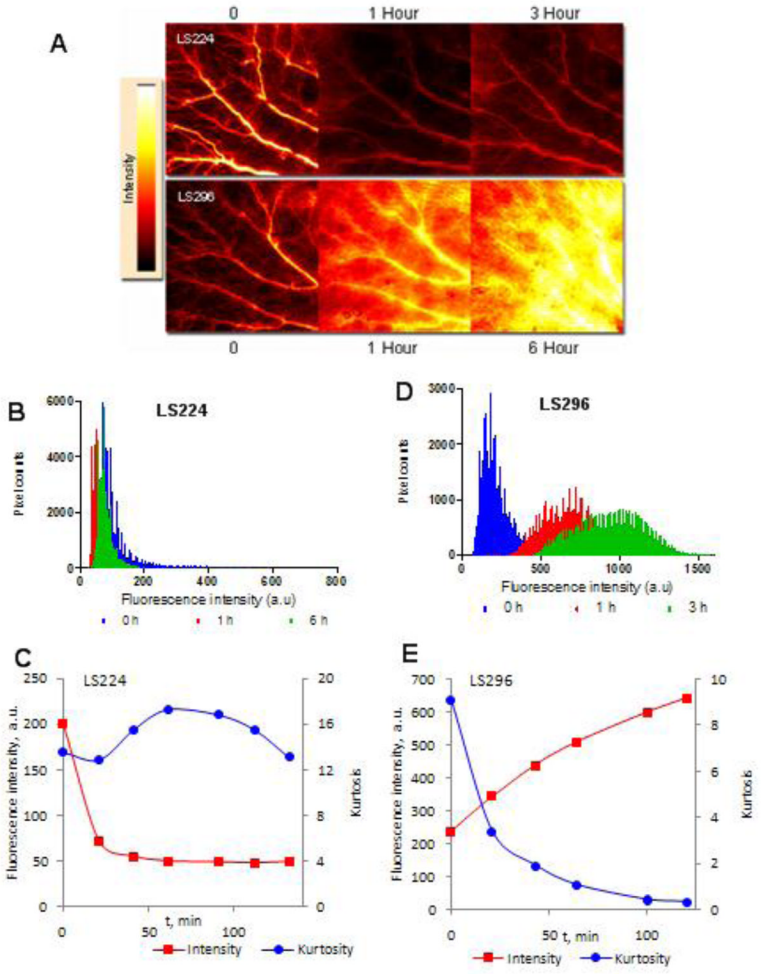

FIGURE 6.

Fluorescence intensity maps at given times after injection of LS224 and LS296 (***A***) showing the disparate extravasation and kinetics of the compounds, ex/em 780/800 nm. Fluorescence values at different pixels for calculating kurtosis showed no significant change in the shape (***B***) for LS224 and therefore no changes in kurtosis (***C***) over 6 h while dramatic changes occurred in peak shape (***D***) and kurtosis (***E***) for LS296 within 3 h.

TABLE 1

Binding constants of fluorophores and fluorophore-conjugates to BSA in PBS buffer obtained from fluorescent quenching of tryptophan

Entry	Dye peptide sequence	*K*, M^{-1}
GRDSPK	NH_2-Gly-Arg-Asp-Ser-Pro-Lys–OH	<5,000
LS39 (Cypate-GRDSPK)(33)	Cypate-Gly-Arg-Asp-Ser-Pro-Lys-OH	76,000
LS224 (Cypate-octreotate)(34,35)	Cypate-DPhe-Cyclo(Cys-Tyr-DTrp-Lys-Thr-Cys)-Thr-OH	51,000
LS167 (Cypate-cRGD)(33)	Cypate - cyclo (Arg-Gly-Asp-DPhe-Lys)	56,000
LS296 (LS276-octreotate)	LS276-DPhe-Cyclo(Cys-Tyr-DTrp-Lys-Thr- Cys)-Thr-OH	14,880